ELSEVIER

Ceramics International 29 (2003) 159–168

CERAMICS INTERNATIONAL

www.elsevier.com/locate/ceramint

Sintering of cordierite based materials

M.A. Camerucci[a,*], G. Urretavizcaya[b], A.L. Cavalieri[a]

[a]*Instituto de Investigaciones en Ciencia y Tecnología de Materiales, (INTEMA), Universidad Nacional de Mar del Plata-CONICET, Juan B. Justo 4302 (7600) Mar del Plata, Argentina*

[b]*Centro Atómico Bariloche, Bustillo km 9,5 (8400) S. C. de Bariloche, Argentina*

Received 12 December 2001; received in revised form 2 January 2002; accepted 12 May 2002

Abstract

The sintering behavior of cordierite based materials obtained from powders with different granulometric characteristics (single fractions and binary granulometric mixtures) has been studied. Commercially available cordierite powder was used to prepare these materials by attrition milling, uniaxial pressing and sintering at 1450 °C. The employed cordierite powders were classified as coarse, medium and fine single granulometric fractions. Binary mixtures of them with 30, 50 and 70 wt.% of the smaller component were prepared. Densification degree and kinetics of sintering were studied through density measurements and microstructural analysis (SEM). Phases were determined by XRD and FTIR techniques and examining the isothermal section at the Al_2O_3–SiO_2–MgO system at sintering temperature. The contact angle of the glassy phase present at this temperature was measured using the heating microscopy technique. The characteristics of the starting powders and the particle packing were correlated to the developed microstructures and a sintering mechanism was proposed.

Keywords: A. Sintering; B. Microstructure; D. Cordierite; D. Mullite

1. Introduction

Cordierite ($2Al_2O_3.5SiO_2.2MgO$) is a technically important ceramic which is applied in a great variety of areas. Cordierite and cordierite based glass ceramics, well known because of their low dielectric constant, high resistivity, elevated thermal and chemical stability and very low thermal expansion coefficient, are promising materials for electronic applications. Due to its lower processing costs and its better electrical properties, cordierite is an alternative material to be used as substrate in replacement of alumina, conventionally employed in the electronic industry [1–3]. Cordierite ceramics present a very narrow sintering temperature range and they are not easily sintered without any sintering aids in order to operate a liquid-phase process close to their melting point (1460 °C). Some attempts have been made to improve the sinterability of cordierite. These studies mainly point to both the use of sintering aids [4,5] and the development of new methods of synthesis [6,7]. Unfortunately, these possible solutions can produce deleterious effects on the thermal and electrical properties of cordierite [8,9] increasing the processing costs.

The aim of this paper is to study the sintering behaviour of cordierite based materials when particular packings are tailored by control of the granulometric characteristics of the starting powders.

2. Experimental procedure

2.1. Starting powder characterization

A commercially available cordierite (CORCR Baikowski, France) was used as the starting powder. Its mean particle size ($D_{50} = 1.82$ μm) and specific surface area BET ($S_S = 3.4$ m^2/g) were measured using a Coulter LS 130 analyzer with Dolapix PC33 as deflocculant and a Monosorb Quantachrome equipment, respectively. The impurity level determined by wet chemical analysis was less than 0.17 wt.% (Table 1). The real density of cordierite powder ($\delta_{R\ cordierite} = 2.6$ g/cm^3) was determined by kerosene picnometry. An heterogeneous cordierite powder morphology composed by flat and/or

* Corresponding author. Fax: +54-223-4810046.
E-mail address: andcamer@fi.mdp.edu.ar (M.A. Camerucci).

0272-8842/03/$22.00
PII: S0272-8842(02)00100-1

Table 1
Wet chemical analysis of as-received cordierite powder (wt.%)

Al_2O_3	SiO_2	MgO	Fe_2O_3	TiO_2	CaO	Na_2O	K_2O	W.L. (1000 °C)
36.9	49.4	12.32	0.03	0.013	0.10	0.02	0.004	0.004

rod-like submicronic particles together with some bigger ones was observed by scanning electron microscopy [10]. It is possible that some of the particles are not single-grain, but aggregates of small grains. However, this fact could be discard taking into account some experimental data: the measured density of the material was close to that of cordierite and the value of its specific surface area was in the typical range of dense particles.

The composition of the starting material was located in the Al_2O_3–SiO_2–MgO ternary system [11]. For this purpose, just the amounts of silica, alumina and magnesia of the cordierite powder were considered, adding the percentage of CaO to that of MgO. This assumption can be made because of the low level of CaO (0.1 wt.%) and the possibility of the formation of a solid solution between cordierite and calcium up to 4.7 wt.% [12,13]. For these weight percentages ($SiO_2 = 50\%$, $Al_2O_3 = 37\%$ and $MgO = 13\%$), the composition of the starting cordierite powder was located in the crystallisation field of mullite shifted to the alumina corner from the cordierite stoichiometric composition ($SiO_2 = 51.4\%$, $Al_2O_3 = 34.8\%$ and $MgO = 13.8\%$), in the cordierite-mullite-silica compatibility triangle. So, the calculated weight percentages of these phases were 92% cordierite, 7% mullite and 1% silica. The difference between the real density of the starting cordierite powder ($\delta_{R\ cordierite} = 2.6\ g/cm^3$) and that of the stoichiometric one ($\delta_{th\ cordierite} = 2.52\ g/cm^3$) was attributed to the presence of mullite of greater density ($\delta_{th\ mullite} = 3.16\ g/cm^3$). XRD powder patterns of the as-received powder were recorded with a Philips X-ray diffractometer using the Cu K_α radiation and a Ni filter. FTIR spectra was obtained employing a Bruker IFS25 infrared, using the KBr pellet technique. α-cordierite (JCPDS Powder Diffraction Data Card Nº 13–293) was identified as the major phase and mullite as the secondary one (JCPDS Powder Diffraction Data Card Nº 15–776) by XRD and FTIR, while silica was not determined using these techniques [14,15]. Differential thermal analysis (DTA) was carried out in air at a heating rate of 10 °C/min up to 1450 °C with alumina as reference employing a Shimatzu DTA-50 equipment. The onset of an endothermic peak was observed at 1400 °C attributed to the liquid formation (in the ternary system, the invariant point located at 1355 °C is the lowest temperature at which a liquid appears). Thermal shrinkage curve was determined up to 1450 °C at a heating rate of 10 °C/min on prismatic samples uniaxially pressed at 20 MPa without binder, using an Adamel Lhomargy dilatometer. Up to 850 °C the thermal expansion of the lattice was observed (0.2%), a small value in agreement with the very low thermal expansion coefficient of cordierite materials. From 850 °C, the shrinkage by sintering starts to be evident with increasing rate from 1350 °C when a liquid is formed.

2.2. Green compact preparation

As-received cordierite powders were attrition-milled at 1045 rpm in a mill with a stainless-steel chamber coated with Teflon, using alumina balls (1–2 mm in diameter) as grinding media in isopropyl alcohol. The ball to powder weight ratio was 0.2 (0.33 vol/vol) [16].

Several milling times were selected to obtain the particle size distributions of the single fractions used to prepare the binary mixtures. The powder with the as-received granulometry was taken as the coarse C ($D_{50} = 1.82$ μm; $S_S = 3.4\ m^2/g$) and powders 8 and 32 h milled as the medium M ($D_{50} = 0.9$ μm; $S_S = 6.5\ m^2/g$) and fine F ($D_{50} = 0.45$ μm; $S_S = 11.2\ m^2/g$) single fractions, respectively. The binary mixtures F/C, M/C and F/M were prepared with 30/70, 50/50 and 70/30 weight ratios.

Powder mixtures were homogenized by attrition milling using alumina media in isopropyl alcohol at 1045 rpm for 10 min; dried in an electrical furnace at 80 °C for 24 h and sieved through 400 mesh (37 μm). Pellets with a thickness (0.3 cm) to diameter (1.2 cm) ratio equal to 0.25 of the resulting cordierite powders were uniaxially pressed at 20 MPa without binder employing a lubricated steel cylindrical mold. In these conditions, the friction and the pressure gradients in the compacts are diminished [17] with the consequent increment in density and homogeneity.

Green densities (δ_G) were determined by weight and volume measurements and the relative density percentages (% δ_G/δ_R) were calculated using $\delta_{R\ cordierite} = 2.6\ g/cm^3$. The porosity ($P = 100\text{-}\%\ \delta_G/\delta_R$) was taken as a measure of the particle packing.

2.3. Sintering

In order to enhance the sintering of cordierite by a liquid-phase process avoiding the addition of sintering aids, a previous analysis of the possible present phases at different temperatures was accomplished. The isothermal sections at 1350, 1450 and 1470 °C [11] and at 1400 °C [18] at the Al_2O_3–SiO_2–MgO system were examined in order to select the sintering temperature of the cordierite materials. Samples were sintered in an electric furnace with $MoSi_2$ heating elements at 1400 and 1450 °C for times ranging from 10 min to 8 h. A slow firing schedule selected considering the thermal shrinkage curve (see Section 2.1) was followed: heating

rate of 25 °C/min up to 800 °C and 5 °C/min up to sintering temperature; cooling rate of 10 °C/min up to 800 °C and free cooling up to room temperature.

The apparent densities of the sintered materials (δ_S) were measured by the Archimedes method in distilled water being the error of δ_S determinations 0.7%. The relative density percentages (% δ_S/δ_R) were calculated using the real densities (δ_R) of the powder treated at 1400 and 1450 °C. These last values were obtained considering the parallel mixing rule. For calculations, the percentages of each phase (cordierite, mullite and liquid) determined by examining the isothermal sections of the Al_2O_3–SiO_2–MgO system at 1400 and 1450 °C, theoretical densities of the crystalline phases ($\delta_{th\ cordierite} = 2.52$ g/cm^3 and $\delta_{th\ mullite} = 3.16$ g/cm^3) and picnometry densities of both liquids ($\delta_{pic.\ glass\ 1400\ °C} = 2.47$ g/cm^3 and $\delta_{pic.\ glass\ 1450\ °C} = 2.51$ g/cm^3) were considered. These glassy phases were produced by melting the appropriate amounts of the constituents in a platinum crucible at 1600 °C for 2 h, followed by quenching in water.

The surfaces of the sintered materials were polished with diamond paste from 6 to 1 μm and thermally etched (1400 °C, 30 min with a heating rate of 20 °C/min) in order to observe their microstructures by SEM. Image analysis (Image-Pro Plus software) was used to measure the average grain sizes on the SEM photographs (about 200–300 grains/sample were counted).

3. Results and discussion

3.1. Particle packing

The granulometric distributions of binary mixtures were obtained considering the particle size distribution of single fractions and their characteristic parameters (mean diameter, D_{50} and width, W) were calculated. The expression $W = D_{80} - D_{20}/D_{50}$ where D_{80}, D_{20} and D_{50} are the diameters corresponding to 80, 20 and 50 vol.% particles, respectively, was taken as a measure of the particle size distribution width.

In order to analyze the packing degree obtained with the different single granulometric fractions and their binary mixtures, the morphology of the particles in addition to the characteristic parameters of particle size distributions and the porosity (Table 2) were considered.

Different porosity values were obtained with the single fractions. Since the packing of spherical monosize particles gives equal porosity independently of its size, differences in porosity can be explained considering that the particles are not totally spherical (as it was observed by SEM) and they are not monosize. For all the fractions (C, M and F) a value of $\ln \sigma = D_{84}/D_{50} > 0.5$ is calculated, and when the logarithm of the standard geometrical deviation results > 0.5, the powder is not considered to be composed by monosize particles [19].

Table 2
Mean diameter (D_{50}) and width (W) of particle size distributions, green densities (δ_G) and porosities of green materials (% P); final densities (δ_S) and densification degrees (% δ_S/δ_R) sintered materials

Materials	D_{50} (μm)	$W = (D_{80} - D_{20}/D_{50})$	δ_G (g/cm^3)	$\%P = (100 - \delta_G/\delta_{pic})$	δ_S (g/cm^3)	% (δ_S/δ_R)
C	1.82	1.50	1.44	44.60	2.42	94.16
M	0.90	0.90	1.50	42.30	2.49	96.89
F	0.45	1.50	1.52	41.15	2.50	97.27
F/C 30/70	1.10	1.80	1.53	41.15	2.40	93.39
M/C 30/30	1.35	1.50	1.47	43.50	2.38	92.61
F/M 30/70	0.80	1.20	1.52	41.50	2.41	93.77
F/C 50/50	0.90	1.80	1.58	39.20	2.46	95.72
M/C 50/50	1.20	1.20	1.50	42.30	2.48	96.50
F/M 50/50	0.70	1.20	1.54	40.80	2.49	96.89
F/C 70/30	0.70	1.60	1.55	40.40	2.50	97.27
M/C 70/30	1.00	1.10	1.50	42.30	2.45	95.33
F/M 70/30	0.60	1.00	1.54	40.80	2.52	98.05

The lower porosity (better packing) was obtained with the F fraction. The wider particle size distribution of F and its more regular particles originated by milling during longer time justify that F fraction packed better than M. However, the C fraction with a particle size distribution width similar to F ($W = 1.50$), showed the worst packing. This behavior was attributed to the irregular flat morphology of coarse particles in comparison with fine ones, which had been rounded by the milling effect. This feature has influence in the packing as much as in the pressing process [17].

The particle packing of the binary mixtures resulted equal or better than that of the single fractions. This was expected as a consequence of the replacement mechanism, that results by the interaction of the two granulometric components, in which the size ratio plays one of the most significant roles [20]. The porosities of the binary mixtures as a function of the percentage of the smaller components are shown in Fig. 1. In the

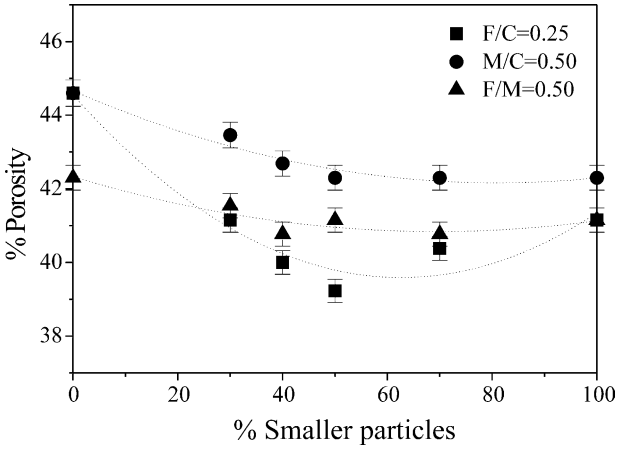

Fig. 1. Percentage of porosity (% P) of single fractions and binary mixtures as a function of the smaller particle content.

intermediate composition range (30/70; 50/50 and 70/30), the more effective packing was achieved with the F/C mixtures. This fact was attributed to the smaller size ratio (D_{50} fine/D_{50} coarse = 0.25) and higher width (W) of the granulometric distributions. For the F/M and M/C mixtures with similar size ratios (0.5) and distribution width ($W = 1.20$), the best packing was attained in F/M mixtures. This was associated to the less irregular shape of the particles of F fraction compared with C particles in the M/C mixture. In the F/C binary mixture, the minimum porosity occurs at a composition about 50 wt.% of the smaller component. For M/C and F/M mixtures, the minimum porosity spreads over a range of compositions.

3.2. Selection of the sintering temperature in the Al_2O_3–SiO_2–MgO system

In order to select the sintering temperature, the composition of the starting material ($SiO_2 = 50\%$, $Al_2O_3 = 37\%$ and $MgO = 13\%$) was located in the isothermal sections at 1350, 1450 and 1470 °C [11] and at 1400 °C [18] at the Al_2O_3–SiO_2–MgO system (Fig. 2) and the present phases were determined. At 1350 °C, the composition of the starting material was located in the cordierite-mullite-silica compatibility triangle. Due to the absence of glassy phase it will be difficult to sinter the cordierite compacts. From 1400 °C, composition areas completely melted or solids in equilibrium with liquids are present. At 1400 and 1450 °C, the composition of the starting cordierite powder was located in the crystallization field of mullite, in the cordierite-mullite-glass compatibility triangle close to the cordierite stoichiometric composition ($SiO_2 = 51.4\%$, $Al_2O_3 = 34.8\%$ and $MgO = 13.8\%$). The present phases were cordierite, mullite and glass, and the calculated weight percentages depended on the treatment temperature. The obtained values were 89% cordierite, 9% mullite and 2% glass for 1400 °C and 84% cordierite, 10% mullite and 6% glass for 1450 °C. In addition, at both temperatures the liquids differed in

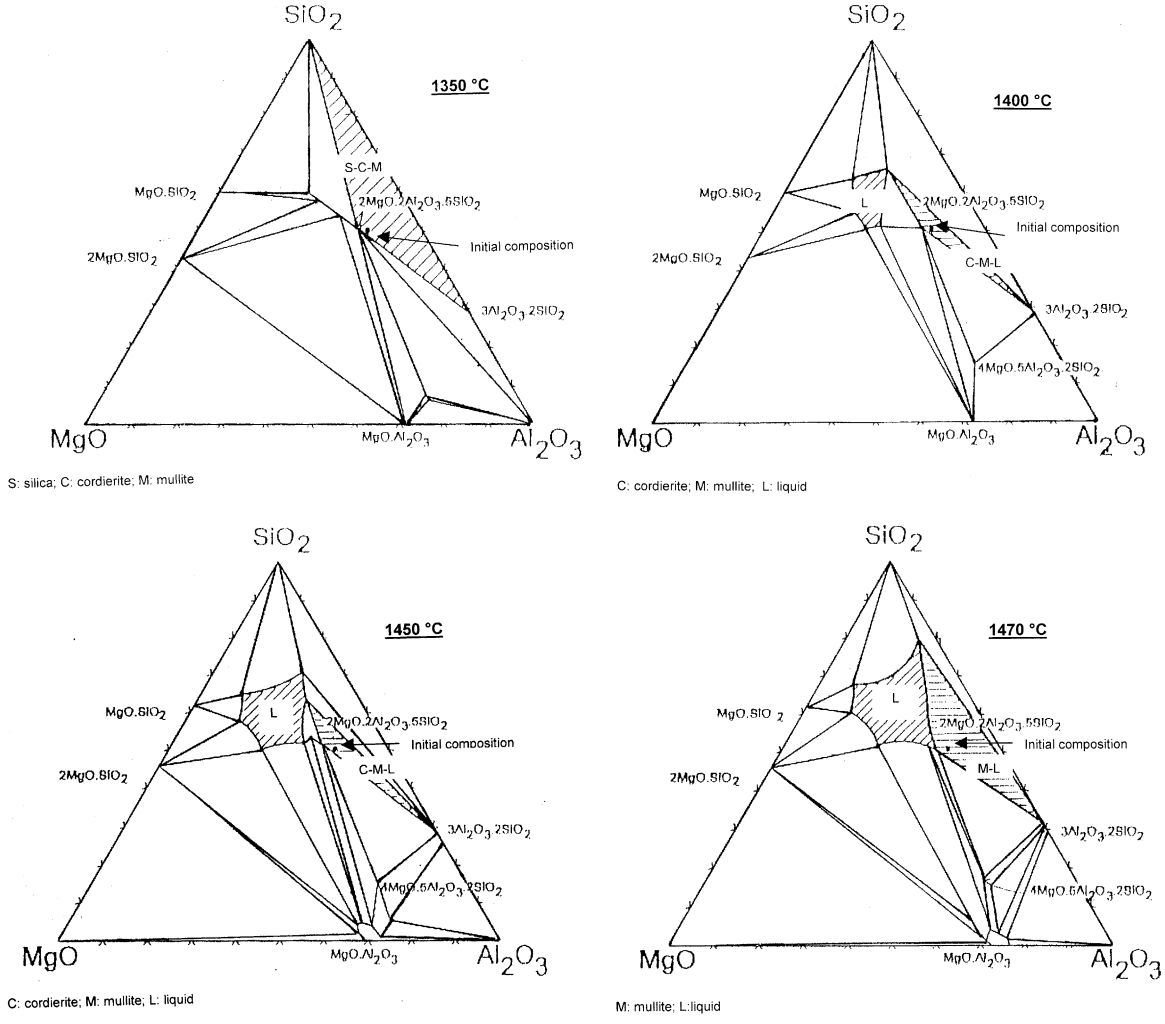

Fig. 2. Localization of the starting material in the isothermal sections at 1350, 1400, 1450 and 1470 °C at the Al_2O_3–SiO_2–MgO system.

composition: 64% SiO_2, 20% Al_2O_3 and 16% MgO at 1400 °C and 63% SiO_2, 25% Al_2O_3 and 12% MgO at 1450 °C. At 1460 °C, the stoichiometric cordierite incongruously melts to form mullite and a liquid [11]. At 1470 °C, the composition was located in the zone of coexistence of mullite and a liquid.

From this analysis, it results evident that the temperature range of sintering is very narrow. Two possible sintering temperatures for these cordierite materials were selected: 1400 and 1450 °C.

The crystalline phases (cordierite and mullite) were confirmed by XRD and FTIR in samples treated at 1400 and 1450 °C, 2 h. In the XRD diagrams of cordierite powders calcined at both temperatures the complete pattern of α-cordierite can be seen together with some mullite peaks (16.4; 25.9; 26.3; 33.4; 35.3; 40.9°2θ) of low intensity. The interval between 25 and 27°2θ was analyzed due to the overlap of the more intense, double peak of mullite [(120) and (210) lines] and a cordierite peak (112) of significant intensity. The asymmetry of the peak supports the presence of mullite. By FTIR, the characteristic bands of cordierite together with some mullite peaks were identified, confirming the results obtained by X-ray diffraction. A sharp band with an intense absorption at 780 cm^{-1} (ring structure of SiO_4 tetrahedra); a peak at 1120 cm^{-1} belonging to the Si–O stretching vibration; sharp bands of lower intensity at 584, 634 and 695 cm^{-1}; a broader peak at 1178 cm^{-1} and a wide band at 956 cm^{-1} were observed [14,20,21]. Also, a shoulder was observed at 1140 cm^{-1} in the band at 1178 cm^{-1} that can be attributed to overlap of the double peak at 1164 and 1137 cm^{-1} (Al–O and O–Al–O stretching vibration of the tetrahedral bonds of mullite or corresponding to Si–O–Al bonds). Two peaks at 746 and 565 cm^{-1} (Al–O tetrahedral and Al–O octahedral bonds of mullite, respectively) appeared overlapped with cordierite bands [15,22,23]. Also, the shifting towards lower frequencies of the cordierite band between 790 and 980 cm^{-1} that occurs in presence of mullite was observed [24].

The densification degree (% δ_S/δ_R) achieved in cordierite samples (coarse fraction) treated at 1400 and 1450 °C during 2 h was determined. At 1400 °C a significative densification (66.41%) was not observed while at 1450 °C a higher densification degree (94.16%) was achieved in agreement with the notable diminution of the porosity observed by SEM. This behavior can be partially explained because of the higher amount of liquid at 1450 °C that favors the sintering mechanism in presence of a liquid phase. Other factors such as the viscosity and the wetting angle of the glassy phase at the sintering temperature will be analyzed in detail in a future work [25].

From the results of the analysis of the Al_2O_3–SiO_2–MgO system and the densification degree given above, the selected sintering temperature was 1450 °C [18].

3.3. Densification degree

In order to calculate the densification degree of the materials, the real density of the powder treated at 1450 °C, 2 h was obtained by the parallel mixing rule ($\delta_R = 2.57$ g/cm^3) and confirmed by kerosene picnometry. The densification degree (% δ_S/δ_R) of the sintered materials was calculated as the ratio between the apparent (δ_S) and the real (δ_R) densities (Table 2).

The densification degree of cordierite materials strongly depends on both the particle size distribution features and the particle shape of the starting powders and it is also related to the effectivity of their packing [26,27].

The densification degree of the single fractions increases in the order C < M≈F (94.16–97.27%) in agreement with the increment in their green densities (1.44–1.53 g/cm^3) (Table 2). It can be seen that the materials with the lowest mean particle diameters, F and M ($D_{50} = 0.45$ and 0.92 μm, respectively) reached higher densities than C, which exhibited greater mean particle size ($D_{50} = 1.82$ μm). Additionally, the progressive change in the particle shape by the increasing powder milling times also contributed to the higher final densities of F and M.

However, regarding the densification degree of the binary granulometric mixtures, a simple order was not obtained. Not always the best green densities produced the higher final densities of the sintered materials. In every binary mixture with 30 wt.% of the smaller particles, the obtained densities were lower than those reached with the materials prepared with the single fractions. Conversely, in the mixtures with 50 and 70 wt.% of the smaller granulometric fraction, the final densities resulted similar or greater than those of the single fractions. The lower porosity was reached for the binary mixture of fine and medium particles with the higher amount of the smaller ones F/M 70/30 wt.%. This major contribution to the densification by sintering in comparison with the other binary mixtures can be related to the addition of two factors: presence of more regular particles due to the grinding effect that allow a more effective green packing and diminution of the mean particle size of its binary granulometric distribution in relation to the mean diameters of both F and M single fractions distributions.

3.4. Microstructure

In Fig. 3, SEM photographs of the sintered (1450 °C, 2 h) single fractions (C, M and F) and their 50/50 binary mixtures (C/F, M/C and F/C) are shown.

The microstructures resulted rather homogeneous with mainly equiaxial grains of similar submicronic sizes and few spherical pores with sizes close to grain ones. In single fractions, the mean grain sizes ($D_{mean}C = 0.46$ μm;

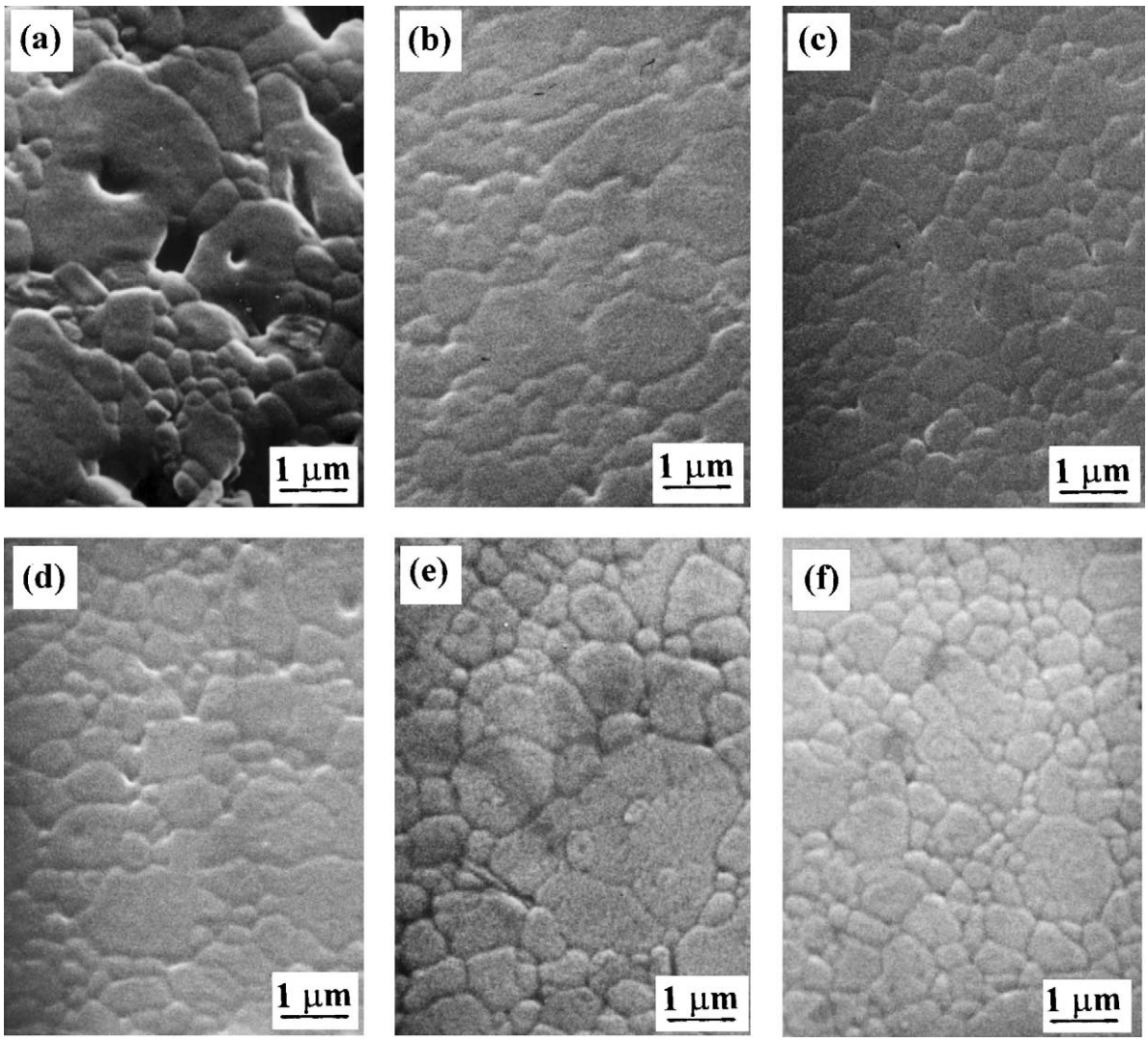

Fig. 3. SEM photographs of materials sintered at 1450 °C, 2 h: (a) C, (b) M, (c) F, (d) F/C 50/50, (e) M/C 50/50 and (f) F/M 50/50.

$D_{meam}M = 0.44$ μm and $D_{mean}F = 0.30$ μm) decreased as the initial particle size (Table 2). In the studied binary mixtures the mean grain sizes (D_{mean}) resulted very similar between them and in the same range (0.45–0.33 μm) as single fractions. It is worthy to note that the D_{mean} was always smaller than the initial particle size even for the powder F with the finest particles ($D_{50} = 0.45$ μm) in which the lowest grain size was obtained ($D_{mean} = 0.30$ μm). Elongated grains attributed to the second phase (mullite) were observed in some materials, these grains presented an aspect ratio ≈1.9.

The binary material F/M presented the most homogeneous microstructure with the narrowest grain size distribution. The homogeneity of the materials obtained from single fractions following the order C < M < F in agreement with their grain size distributions. By comparison with every binary mixture, C presented the lowest homogeneity while M and F showed microstructures with similar homogeneity as the most homogeneous binary one (F/M).

3.5. Sintering mechanism

Several facts, as present phases (cordierite, mullite and glass); final densities; developed microstructures (porosity, grain sizes); relatively high amount (6 wt.%), contact angle and viscosity of the glassy phase at sintering temperature, allow us to assume that the liquid-phase mechanism of sintering operates in the cordierite sintering conditions studied in the present work.

Additionally, experimental results (DTA and dilatometric curves, Section 2.1) support the possibility of occurrence of this mechanism. The onset of an endothermic peak at 1400 °C, attributed to the formation of liquid, was registered in the thermal analysis. Furthermore, an increment of the shrinkage rate at 1350 °C was

observed in dilatometric measurements and attributed to a change in the mechanism, operating a sintering in presence of a liquid phase. The very slow shrinkage rate up to 1350 °C was associated to a solid-state sintering. The microstructures described above will be examined in order to understand the mechanism of densification.

Assuming that a liquid-phase sintering mechanism is operating and considering that the grain sizes in the sintered samples result smaller than the initial particle sizes it can be inferred that the particle-particle rearrangement takes place. Moreover, from the similarity of the mean grain sizes observed in every material it could be inferred that the size of the produced fragments has an insignificant dependence on both the morphology and the mean diameter of the starting particles.

The rearrangement can proceed in two steps. In the first one, the densification occurs rapidly as soon as the liquid phase is formed. Pores are filled and the particles are rearranged due to capillary pressure resulting in a closer packing. The second step involves particle fragmentation and subsequent repacking of the fragments. The magnitude of the rearrangement force is a function of particle size, pore size, contact angles, particle morphology and liquid phase content [26,28].

At the sintering temperature, the contact angle values of the liquid phase on both cordierite and mullite substrates were $\theta = 18^\circ$ and $\theta = 23^\circ$, respectively and its viscosity resulted equal to 1.3×10^2 Pa.s. The relatively high contact angles could limit the complete penetration of the boundaries by the melt unless a great amount of liquid is present as it occurs in our system (6 wt.% glass). The higher viscosity of the liquid, the higher the amount of liquid phase needed for the rearrangement of particles due to the fact that its spreading out is retarded. The high viscosity and the low surface energy of the siliceous liquid as the studied one limit both the capillary pressures at the contact points of the wetted particles and the coefficient diffusion [28]. Due to the last factors, it is suggested that the contribution of solution-reprecipitation events (secondary stage in which the densification mainly occurs through particle morphology accommodation, the dissolution of small particles and precipitation over the larger ones) to the densification mechanism should be minor. This possibility was further verified by examining the developed microstructure.

3.6. Kinetics of densification

The kinetics of densification of the coarse single fraction and the 50/50 wt.% binary mixtures was studied. In Fig. 4, the change in the densification degree was plotted as a function of time of permanence at sintering temperature.

A significant increment in the densification degree was determined up to 2 h. From this time, no variation in the 'final density' values was registered. As would be expected for a liquid-phase sintering, the densification in these materials was very fast once the liquid was formed. After treatment at 1450 °C, binary mixtures (at 10 min) and coarse single fraction (at 30 min) had already reached about 95 and 80% of the theoretical density, respectively. In F/C, M/C and F/M materials treated during 2 h at the same temperature, the final densities differed between them about 1%. The higher value was achieved in the F/M material (96.89%) and the lower one was obtained in the C material (94.16%): with a smaller mean particle size as in the case of the F/M material ($D_{50} = 0.7$ μm), the rearrangement was favored and the final density was higher.

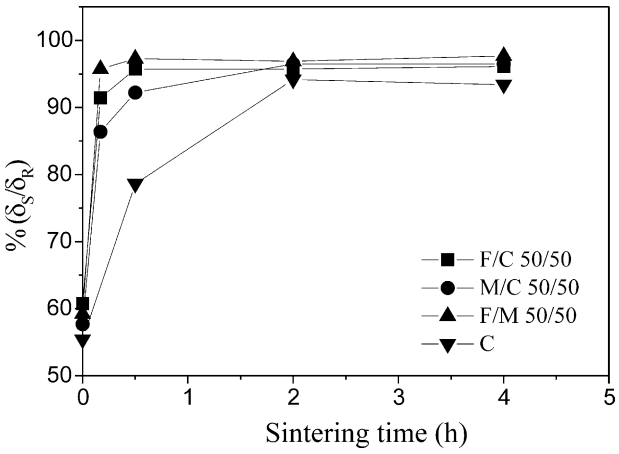

Fig. 4. Densification degree achieved in C and F/C, M/C, F/M 50/50 materials sintered at 1450 °C as a function of the sintering time.

Furthermore, differences in the 'densification rates' were observed. In regard to the binary mixtures, the F/M presented the highest shrinkage rate while the M/C was the material which sintered more slowly: after 30 min at 1450 °C, F/C and F/M achieved the densification limit while this value was just attained at 2 h in M/C and C materials.

It must be noted that every binary mixture sintered much more rapidly than the single fraction C which has the lower packing density. In general, the less effective initial packing reduces the densification rate while it improves the final density. The packing effectiveness or relative density of the green compacts (% δ_G/δ_R) influences on the sintering rate. As the green density increases, there is more mechanical interlocking and less amount of the pore phase. Consequently, the liquid cannot flow into the surrounding pores and the capillary force responsible for rearrangement is reduced [26]. So, a possible explanation for the lower densification rate of C in relation to binary materials could be given by considering the influence of the mean particle sizes and their shapes besides the packing effectiveness. Each granulometric mixture has particles with small mean size ($D_{50\ F/C} = 0.9$ μm, $D_{50\ F/M} = 0.7$ μm, $D_{50\ M/C} = 1.2$ μm) and more

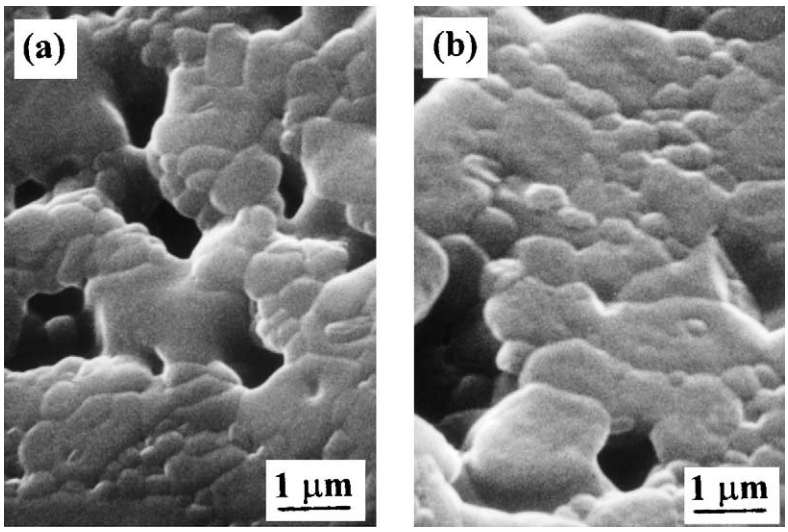

Fig. 5. SEM photographs of C material sintered at 1450 °C during: (a) 30 min and (b) 4 h.

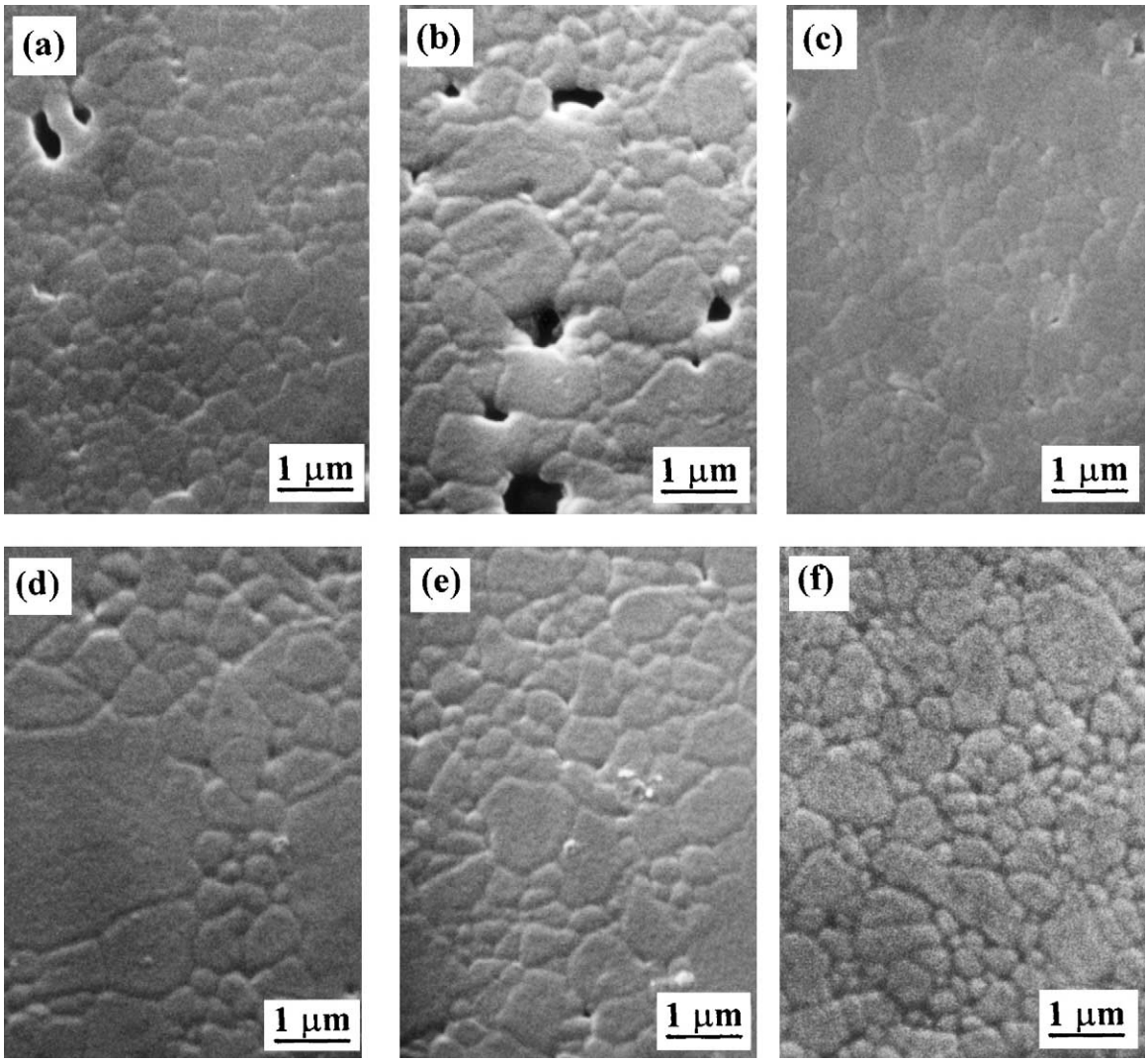

Fig. 6. SEM photographs of materials sintered at 1450 °C during: 10 min (a) F/C 50/50, (b) M/C 50/50 and (c) F/M 50/50 and 4 h (d) F/C 50/50, (e) M/C 50/50 and (f) F/M 50/50.

regular and smooth shape in respect of the large ($D_{50} = 1.82$ μm) irregular and flat particles of the single fraction C. Both factors could be enhancing the densification rate in binary materials in spite of a more effective packing when the sintering mechanism by a liquid-phase process is operating since the rearrangement can be aided by small smooth particles [25].

SEM photographs of the single fraction C sintered during 30 min and 4 h and binary mixture materials sintered for 10 min and 4 h are shown in Figs. 5 and 6, respectively. In Fig. 3, the microstructure of the samples sintered during 2 h were showed before.

In C sample, a high porosity can be observed at 30 min, and a coarsening of the mean pore size is detected when the time of the thermal treatment increases. This pore coarsening can be attributed to particle rearrangement. The mean pore size increases even as the total porosity decreases because of the shrinkage by sintering. With respect to materials obtained from the binary granulometric mixtures thermally treated during 10 min, higher porosity was observed in the order F/M < F/C < M/C in agreement with the measured final densities. After 2 h (Figs. 3d–f) and 4 h (Fig. 6) at 1450 °C, a significant difference in the developed microstructures was not appreciated. In every material, similar grain sizes with a slight increment in those obtained after 4 h was observed. As it was already mentioned, the more homogeneous microstructures with the narrowest grain size distributions corresponded to F/M at every sintering time.

After 10 min of thermal treatment at 1450 °C it can be inferred that the densification by secondary rearrangement of the particle fragments is already operating due to the fact that the observed mean grain sizes were always smaller than the starting mean particle sizes and some densification had occurred. Also, the porosity observed at 2 h in every material is notably lower in agreement with the measured final densities.

Additionally, it is interesting to note that a significant grain growth did not occur (Table 3) neither a change in the morphology of the grains (Fig. 3), supporting the assumption that little or no dissolution and precipitation takes place during densification.

Table 3
Grain mean diameters (μm) of the coarse single fraction and 50/50 binary mixtures sintered at 1450 °C

Sintering time (min)	C (μm)	F/C 50/50 (μm)	M/C 50/50 (μm)	F/M 50/50 (μm)
10	–	0.37	0.37	0.21
30	0.47	–	–	–
120	0.46	0.44	0.42	0.38
240	0.55	0.49	0.45	0.45

– Not determined.

4. Conclusions

In general, the densification degree of the materials was improved by decreasing the mean particle size of starting granulometric distributions or formulating binary granulometric mixtures with more than 50 wt.% of the smaller particles. However, the binary mixtures with the best green densities not always achieved the highest final densities by sintering. The lowest mean particle size of F/M 70/30 wt.% granulometric distribution together with its more regular particle shape were assumed as the more important factors that contributed to the highest densification of this material. In addition, the most homogeneous grain size distribution (the narrowest one) with the small mean grain size was observed in F/M microstructure.

For all materials involved, the grain sizes were smaller than the initial particle ones due to the fact that the particle-particle rearrangement takes place, assuming that a liquid-phase sintering mechanism is operating. On the other hand, neither a significant grain growth with the increasing sintering time nor a change in the morphology of the grains are observed. These facts, in addition to the high viscosity and the low surface energy of siliceous liquids as the studied one, support the fact that few or no events of dissolution-reprecipitation contribute to the mechanism of densification.

In general, the more effective packing reduces the densification rate while it improves the sintered density. However, the coarse commercial material with the lowest green density exhibited the worst sintering behavior achieving the lower final density at the longest sintering times in relation to binary mixtures. The high particle size of the first material and its more irregular shape are two factors that strongly diminish its sintering rate because the rearrangement is aided by small and smooth particles.

References

[1] R.R. Tumala, Ceramic and glass-ceramic packaging in the 1990s, J. Am. Ceram. Soc. 74 (5) (1991) 895–908.
[2] M.A. Subramanian, D.R. Corbin, U. Chowdhry, Better ceramic substrates through zeolites, Bull. Mater. Sci. 16 (6) (1993) 665–678.
[3] S.H. Knickerbocker, A.H. Kumar, L.W. Herron, Cordierite glass-ceramics for multilayer ceramic packaging, Am. Ceram. Soc. Bull. 72 (1) (1993) 90–95.
[4] C.F. Yang, The effect of Bi_2O_3 on the dielectric characteristics of $CaO–Al_2O_3–MgO–SiO_2$ glass ceramics, J. Mater. Sci. 15 (1996) 1618–1620.
[5] S. Lo, C. Yang, The sintering characterisitics of Bi_2O_3 added $CaO–Al_2O_3–MgO–SiO_2$ glass powder, Ceram. Int. 24 (1998) 139–144.
[6] D. Sporn, H. Schmidt, Synthesis of mullite and cordierite powders by sol–gel process and their sintering behaviour, in: G. de With, R.A. Terpstra, R. Metszlaar (Eds.), Euroceramics, Processing of Ceramics, Elsevier Applied Science V1, 1989, pp. 1120–1124.

[7] M.G.M.U. Ismail, H. Tsunatori, Z. Nakai, Preparation of mullite cordierite composite powders by the sol–gel method: its characterisitcs and sintering, J. Am. Ceram. Soc. 73 (3) (1990) 537–543.
[8] M. Awano, H. Takagi, Y. Kuwahara, Grinding effects on synthesis and sintering of cordierite, J. Am. Ceram. Soc. 75 (9) (1992) 2535–2540.
[9] R. Gopi Chandran, K.C. Patil, Combustion synthesis, characterisation, sintering and microstructure of cordierite, J. Br. Ceram. Trans. 92 (6) (1993) 239–245.
[10] M.A. Camerucci, A.L. Cavalieri, R. Moreno, Slip casting of cordierite and cordierite–mullite materials, J. Eur. Ceram. Soc. 18 (1998) 2149–2157.
[11] R.M. Smart, F.P. Glasser, The subsolidus phase equilibria and melting temperatures of $MgO–Al_2O_3–SiO_2$, Ceram. Int. 7 (3) (1981) 90–97.
[12] P. Scardi, N. Sartori, A. Giachello, P.P. Demaestri, F. Branda, Influence of calcium oxide and sodium oxide on the microstructure of cordierite catalyst supports, Ceram. Int. 19 (1993) 105–111.
[13] S. Sundar, V.S.S. Vespa, A.M. Umarji, Effect of substitution of Ca on thermal expansion of cordierite ($Mg_2Al_4Si_5O_{18}$), J. Am. Ceram. Soc. 76 (7) (1993) 1873–1876.
[14] R. Gopi Chandran, K.C. Patil, G.T. Chandrappa, Combustion synthesis, characterization, sintering and microstructure of mullite–cordierite composites, J. Mater. Sci. Lett. 14 (1995) 548–551.
[15] Ph. Colomban, Structure of oxide gels and glasses by infrared and Raman scattering. Part 2: Mullites, J. Mater. Sci. 24 (1989) 3011–3020.
[16] M.A. Camerucci, A.L. Cavalieri, Process parameters in attrition milling of cordierite powders, J. Mater. Synth. Process. 6 (2) (1998) 117–123.
[17] R. Thompson, Mechanics of powder pressing: I: model for powder densification, Am. Ceram. Bull. 60 (2) (1981) 237–243.
[18] M.A. Camerucci, Desarrollo y Evaluación de Materiales Cerámicos de Cordierita y Cordierita-mullita, PhD thesis, Universidad Nacional de Mar del Plata, 1999.
[19] A.S.V. Galakhov, V. Shevchenko, Analysis of two-dimensional packings, Ceram. Int. 18 (1992) 213–221.
[20] H. Kodama, Infrared spectra of minerals. Reference guide to identification and characterization of minerals for the study of soils, Research Branch Agriculture Canadá, 1985.
[21] V.C. Farmer (Ed.), The Infrared Spectra of Minerals, London, 1974.
[22] K.J.D. Mackenzie, Infrared frequency calculations for ideal mullite ($3Al_2O_3.2SiO_2$), J. Am. Ceram. Soc. 55 (2) (1972) 68–71.
[23] H.J. Percival, J.F. Duncan, P.K. Foster, Interpretation of the kaolinite-mullite reaction sequence from infrared absorption spectra, J. Am. Ceram. Soc. 57 (2) (1974) 57–61.
[24] M.G.M.U. Ismail, H. Tsunatori, Z. Nakai, Preparation of mullite cordierite composite powders by the sol–gel method: Its characteristics and sintering, J. Am. Ceram. Soc. 73 (3) (1990) 537–543.
[25] R.M. German, Sintering Theory and Practice, John Wiley & Sons, Inc, New York, 1996.
[26] J.M. Ting, R.Y. Lin, Effect of particle size distribution on sintering. Part II. Sintering of alumina, J. Mater. Sci. 30 (1995) 2382–2389.
[27] J.H. Jean, T.K. Gupta, Liquid-phase sintering in the glass–cordierite system, J. Mater. Sci. 27 (1992) 1575–1584.
[28] T. Ebadzadeh, W.E. Lee, Processing-microstructure-property relations in mullite–cordierite composites, J. Eur. Ceram. Soc. 18 (1998) 837–848.